*Korean J. of Chem. Eng.*, **7**(2) (1990) *126-137*

# FLOW AND DYNAMIC BEHAVIOR OF DILUTE POLYMER SOLUTIONS IN HYDRODYNAMIC CHROMATOGRAPHY

**Myung-Suk CHUN, O Ok PARK* and Jong Kyu KIM****

Department of Chemical Engineering, Korea Advanced Institute of Science and Technology, Seoul 130-650, Korea

*(Received 1 December 1989 • accepted 26 March 1990)*

**Abstract**—Recently, hydrodynamic chromatography (HDC) has become an important probe for determining the molecular size or molecular shape in the sub-micron range. Although a lot of studies on HDC were performed, the clear understanding on the transport behavior of polymer solutions in porous media has not been achieved yet. In this study, the flow and dynamic behavior of polymer molecules in a packed HDC column is fully analyzed by extending the molecular kinetic approach of dilute polymer solution in a *confined geometry* to elucidate the effects of relative *particle sizes* as well as the *flow strength* on the *retention factor* ($R_f$). $R_f$ equation of each simple polymer model was developed, and the numerical simulation was worked out to illustrate the $R_f$ for rigid rod (RR) polymers. Theoretical predictions were in remarkable agreement with our experimental results of xanthan gum and other published data despite of several approximations. Significant size effects were observed, and for RR model the $R_f$ decreased with increasing the flow strength within a particular range. This feature emphasized a transition behavior from weak to strong flow due to the *orientational* effect of xanthan molecules. It should be noted that our major concern is restricted solely to the hydrodynamic force.

## INTRODUCTION

Understanding the flow behavior of polymer solutions in confined geometries is an important problem in both theoretical and practical senses. There are numerous porous media flows in which confining geometries have a great influence on the dynamic behavior of polymer solutions. Examples of this type include chromatographic flow, enhanced oil recovery, and coating flow. Polymer solutions exhibit lots of dramatic effects during such flows through porous media as listed above. By considering these effects one can easily find a common feature in them, which is the *flow induced conformation of polymer chains*, such as stretching behavior of flexible polymers or orientational change for rigid polymers. In order to develop a molecular theory describing the behavior of dilute polymer solutions in flowing systems, very simple idealizations of a macromolecule must be taken. Despite of many kinds of synthetic polymers and biopolymers, they can be divided into two groups: flexible and rigid polymers, which can be modeled as elastic dumbbell (ED) and rigid dumbbell (RD), respectively. Details on the molecular theory of polymeric liquids can be found in the book of Bird et al. [1].

The hydrodynamic interaction effects in steady shear flow of RD suspensions at arbitrary shear rates were first reported by Stewart and Sorensen [2]. Their computation was done by using Galerkin's method, with linear combination of the spherical harmonics as a trial function. A rectilinear Poiseuille flow was considered by Aubert and Tirrell [3] who predicted the existence of migration of polymer chains in such a nonhomogeneous flow field. Stasiak and Cohen [4] also reported calculations for rectilinear Poiseuille flow using the ED and RD models. In their analysis, however, studies have been restricted to the case of an *infinite domain*. Recently, Park and Fuller [5] and Park [6] established the RD model polymer in confined geometries under simple shear flow to consider the proper boundary effect. Although one can perform many of the theoretical analyses with relative ease due

*Correspondence concerning this paper should be addressed to O.O. Park.

**The present address: Samsung Advanced Institute of Technology, KiHung, Korea.

to the simplicity of the molecular models, the clear description to the flow behavior of polymer solutions in porous media has not been achieved.

An isolated polymer molecule flowing down in confined geometries and undergoing Brownian motion will have an average velocity greater than that of the solvent, which was already recognized two decades ago by DiMarzio and Guttman [7]. The ratio of average particle velocity to average fluid velocity is called retention factor ($R_f$, for brevity), which is always greater than one, indicating that on the average, the particles travel through the column faster than the fluid itself. A more sophisticated theory that was later developed by Brenner and Gaydos [8] incorporated a more accurate analysis of hydrodynamic effects and also included the interaction potential between the colloidal particle and the conduit wall. The flow separation of colloidal particles according to size was first achieved by Small [9], who developed an useful experimental technique to analyze the sizes of polystyrene latex particles and named *hydrodynamic chromatography* (HDC, for brevity). In his system, in addition to hydrodynamic exclusion, the electrostatic force between latex particles and supports was an important factor too. A clear and fundamental understanding of the separation behavior in HDC has been developed by several investigators [10-12].

Up to that point, every study was limited to an isotropic molecule so that there was no evidence of the dependence of $R_f$ on the flow strength. However, if an anisotropic molecule is dealt with then it can be expected apparently that the $R_f$ will depend on flow strength due to its orientation alignment along the flow. Separation of anisotropic molecules by HDC has been studied mainly by Prud'homme and his co-workers after the 1980's [13-15]. Size fractionations of high molecular weight polymers, such as xanthan polysaccharide (cf. more precisely speaking, that is *slightly semi-flexible*) and tobacco mosaic virus (TMV) as rigid polymers, and partially hydrolyzed polyacrylamide and dextran as flexible polymers were experimented (in this regard see, e.g., Refs. 13,14), and then the deformation and orientation phenomena in HDC were interpreted semiquantitatively (see, e.g., Ref. 15). In their researches, however, the efficiency of the size fractionation observed was poor due to the too high flow rates used. Moreover, the decreasing tendency of $R_f$ with increasing flow rate in case of TMV, which was so rapid unfortunately that even it looks like impossible to analyze the sizes of rigid polymers with HDC, was detected. Therefore, we shall try to solve the basic problem just including the hydrodynamic effect, and to explain these results as well as quantitatively and clearly to have some idea of the usefulness for HDC technique in case of macromolecule.

A theoretical study closely related to the present work is that of Park and Fuller [5], who reported the dynamic behavior of polymer solution between two parallel plates with simple shear flow. Their results successfully hold the essential feature of flow of dilute polymer solution in confined geometries. By utilizing these results Park also postulated that there were two regimes of different dependences of flow behavior of rigid polymer on flow rates. The purpose of this study is to predict the flow behavior of dilute polymer solution in packed HDC from the simple molecular models and to elucidate, *inter alia*, the effects of arbitrary particle sizes as well as the flow strength on the $R_f$ by extending both the basic concept and theoretical analysis of Park [6]. In addition, we compare the theoretical predictions with our experiments or previously reported data, and then we shall point out distinctly the conclusions from the good agreement. Remarkably, our present work successfully contribute to overcome the restricted approach of previous studies.

## BASIC FORMULATION

Conventional size-exclusion or gel permeation chromatography (GPC) is a well established technique for characterizing molecular weight distributions of polymers [16]. Since 1974, HDC has become an important tool for molecular size analysis in the submicron range. Its method is similar to GPC, but differs in several important respects. A HDC column packed with nonporous packing presents the particles suspended in the carrier solvent with a tortuous path through a large number of capillary-like tunnels.

### 1. Retention Factor

The first modeling step is to reduce the actual three dimensional bed structure of a HDC column to a set of equivalent capillaries as shown in Figure 1. This idealized HDC model shows that large particles are excluded faster from regions near the wall, where axial velocities are small. Thus larger particles move along the capillary at greater average velocity and small retention time. Here the ratio of the average particle velocity ($V_p$) to the average eluant velocity ($V_m$) can be expressed using the separation factor, $R_f$, defined by

$$R_f = \frac{V_p}{V_m} = \frac{t_m}{t_p} \tag{1}$$

where $t_m$ and $t_p$ are eluant elution time and particle elution time, respectively. $V_p$ is determined by measuring the $t_p$, and $V_m$ by measuring the average elution time of a marker species of molecular size (that is, $t_m$).

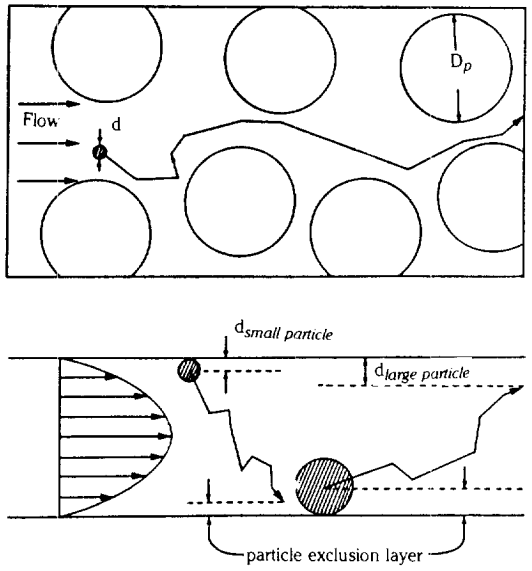


**Fig. 1. Illustration of preliminary modeling steps in HDC.**

The porous media structure of a packed column, displaced at the top, is reduced to the simple capillary model at the bottom.

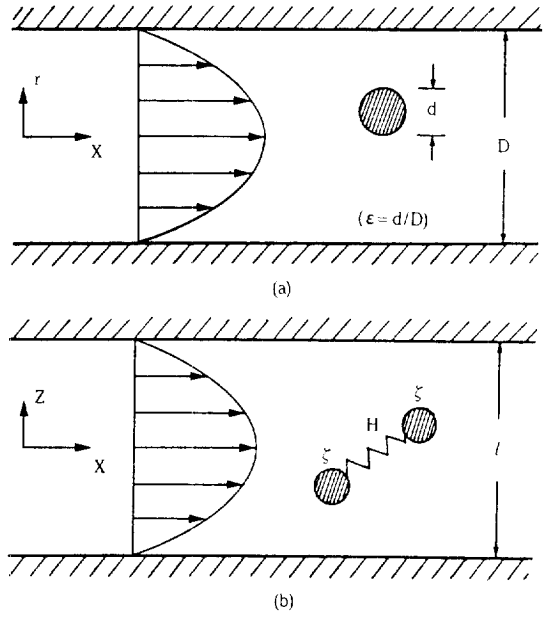


**Fig. 2. The flow field situations for (a) SB model in capillary tube and (b) ED model between two parallel plates.**

For a symmetrical chromatogram, the average residence time corresponds to the peak elution time. Basically if we know the distribution function and velocity profile for particles, then we can calculate the $R_f$ by simple multiplication of these two and then integration over all possible space.

## 2. Single Brownian (SB) Model

Let us suppose that the spherical colloidal particle is an isotropic, that is, single Brownian (SB) model polymer. The $R_f$ of this model polymer in the capillary tube can be estimated from simple arguments based on steric exclusion alone. In SB model, we assume isotropic mass distribution so that there is no term responsible for the alignment of polymer due to the flow. Thus the flow remains Poiseuille velocity profile as far as the flow rate is small. The dimensionless length scale of SB model polymer is defined by $\epsilon = d/D$ as shown in Figure 2a. The local eluant velocity at r and the average eluant velocity can be written in the following forms, respectively,

$$v_m(r) = v_c\left(\frac{1}{4} - r^2\right) \tag{2}$$

$$V_m = \int_0^{1/2} \left(2\pi r \frac{4}{\pi} v_c\left(\frac{1}{4} - r^2\right)\right) dr$$

$$= \frac{v_c}{8}. \tag{3}$$

If the concentration profile is constant the concentration distribution C(r) along the radial axis can be obtained by the normalization condition.

$$C(r) = \frac{4}{\pi} \frac{1}{(1-\epsilon)^2} \qquad (0 \le \epsilon \le 1) \tag{4}$$

Averaging over all radial positions available to the particle, the average particle velocity can be obtained by

$$V_{p,SB} = \int_0^{1-\epsilon/2} (2\pi r C(r)\, v_m(r))\, dr$$

$$= \frac{v_c}{8}(1 + 2\epsilon - \epsilon^2) \tag{5}$$

therefore,

$$R_{f,SB} = -(\epsilon - 1)^2 + 2. \tag{6}$$

Notably, this equation is identical to that achieved by Prieve and Hoysan [10] in their analysis of an equivalent problem. They supposed that, as a limiting case, the role of colloidal forces was negligible, and then recognized the purely hydrodynamic effect.

## 3. Elastic Dumbbell (ED) Model

The simple conceptual model which has been applied most frequently for the study of dilute solutions of flexible polymer chains is the *linear* ED model (cf. [1]). In this ED model, the chain is represented by two beads of hydrodynamic friction and connected by an entropic spring force. In Figure 2b this spring is taken

to be linear with a force constant H and the friction coefficients of each bead $\zeta$. By including the retardation effect of particles, velocity profiles for eluant and particle can be given by the respective expressions

$$v_m(z_c) = v_c\left(\frac{1}{4} - z_c^2\right) \tag{7}$$

$$v_p(z_c) = v_c\left(\frac{1}{4} - z_c^2 - \frac{1}{4}z^2\right). \tag{8}$$

The nondimensionalized equilibrium distribution function which can be derived exactly as described by Aubert and Tirrell [3,17] is given by

$$\psi_{eq}(z, z_c) = C_1 \exp(-a^2 z^2) \tag{9}$$

where

$$C_1 = \frac{a^2}{\sqrt{\pi}\left(a \cdot \mathrm{erf}(a) + \frac{1}{\sqrt{\pi}}(e^{-a^2} - 1)\right)}. \tag{10}$$

Here, length has been scaled by $a' = (2kT/H)^{-1/2}$ and $a = a'/l$ is the reciprocal dimensionless length scale. k and T are Boltzmann constant and absolute temperature, respectively. The probability distribution of center of mass will not be changed by the presence of a one-dimensional flow along the x direction. Therefore, if the flow strength is weak enough to apply the equilibrium distribution function, the $R_f$ of this case can be obtained as

$$R_{f,RD} = \frac{\left(1 - \frac{3}{2a^2}\right)\mathrm{erf}(a) + \left(\frac{1}{a} - \frac{2}{a^3}\right)\frac{1}{\sqrt{\pi}}e^{-a^2} + \frac{2}{a^3\sqrt{\pi}}}{\mathrm{erf}(a) + \frac{1}{a\sqrt{\pi}}(e^{-a^2} - 1)} \tag{11}$$

## 4. Rigid Dumbbell (RD) or Rigid Rod (RR) Model

The model used here is that of the rigid dumbbell (RD) pictured in Figure 3a. This model is the simplest possible description of a rigid polymer and has been used extensively in the interpretation of dilute solutions of such macromolecules. Now we would like to have the appropriate distribution function to elucidate the orientational change, but the exact distribution is not available up to now even though polymers do not disturb the Poiseuille flow. However, the simple shear solution would be very useful because the main orientational change will notably occur near the wall. Therefore, the calculation presented is for the simple shear flow $\vec{v} = \alpha(z,0,0)$ depicted in Figure 3b, where $\alpha$ is the velocity gradient. The conformation of the RD model polymer can be described through a distribution function $\psi(\vec{r}_1, \vec{r}_2)$ which prescribes the probability of the bead location. After defining the bead separation

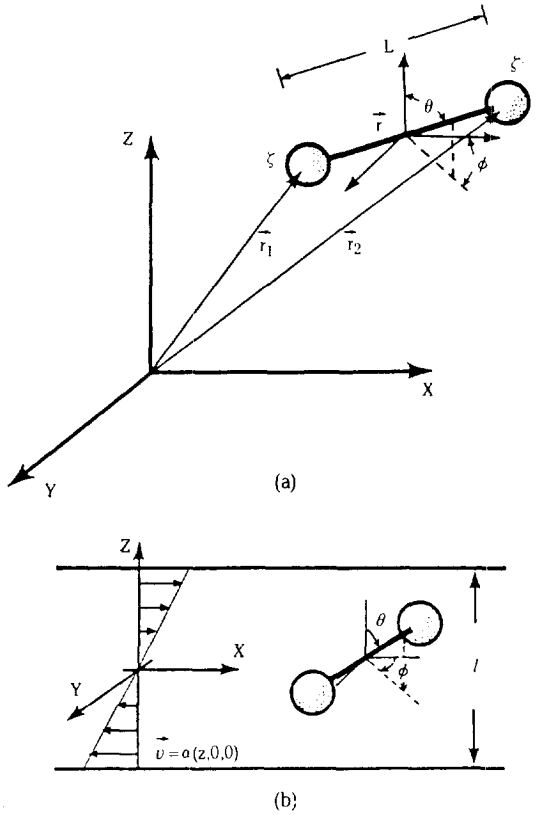


**Fig. 3. The RD model is considered (a) in spherical coordinate system and (b) with flow geometry.**

vector $\vec{r} = (\vec{r}_2 - \vec{r}_1)$ and the center of mass vector $\vec{r}_c = (\vec{r}_1 + \vec{r}_2)/2$, the diffusion equation describing the evolution of the *probability distribution function* $\psi(z_c, \theta, \phi; t)$ can be obtained, where $\theta$, $\phi$ are the polar angles. Figure 3a with the spherical coordinate system is the same situation analyzed by Park and Fuller [5]. The steady state diffusion equation is identical to that used by Stasiak and Cohen [4] and the diffusion equation for $\psi$ has the following form

$$6\frac{\partial \psi}{\partial t} - \beta\Omega\psi + \Lambda\psi + \frac{1}{4}\epsilon^2\frac{\partial^2 \psi}{\partial z_c^2} = 0 \tag{12}$$

with the boundary condition at $z_c = \pm(1 + \epsilon\cos\theta)/2$

$$-\frac{1}{\sin\theta}\frac{\partial \psi}{\partial \theta} \pm \epsilon\frac{\partial \psi}{\partial z_c} = 0 \tag{13}$$

and the normalization condition

$$I(\psi) = 1. \tag{14}$$

Here we have defined the dimensionless velocity gradient $\beta = \alpha/D_r$ and dimensionless dumbbell length

$\epsilon = L/l$, where $D_r = 2kT/\xi L^2$ is the rotational diffusivity, and $l$ is the spacing between the parallel plates. Time has been scaled to the relaxation time of the dumbbell, $\lambda = 1/6D_r$. The operator $\Omega$ due to convection is identical to that used by Stasiak and Cohen [4], and the operator $\Lambda$ is the spherical Laplacian. Equation 14 is simply the conservation of total probability and the normalization operator I can be obtained from the consideration of the restriction placed on the conformation of the RD by boundaries, which was previously defined by Park and Fuller [5].

4-1. *Flows of Arbitrary Strength*

We shall employ the numerical scheme developed by Stewart and Sorensen [2] for the same problem in unbounded flow. The Brownian motion terms of center of mass of the molecules and no flux boundary condition will again be neglected as they do not play any role in space-averaged rheological properties. Equations (12) and (14) can be solved by a series expansion in terms of spherical harmonics:

$$\psi^{2N} = \psi_{eq} \sum_{n=0}^{N} \sum_{m=0}^{2n} (A_{2n}^{m} P_{2n}^{m} C_m) \tag{15}$$

where $A_{2n}^{m}$ is the coefficient of solution which will be determined as a function of $\beta$, $P_{2n}^{m}$ is the associated Legendre polynomial of the first kind and $C_m$ denotes $\cos(m\phi)$. For no flow case, $\psi_{eq}$ can be given by

$$\psi_{eq} = \begin{cases} \dfrac{1}{4\pi} \dfrac{1}{(1-\epsilon/2)} & (0 \le \epsilon \le 1) \qquad (16a) \\ \dfrac{\epsilon}{2\pi} & (\epsilon > 1). \qquad (16b) \end{cases}$$

4-2. *The Galerkin Solution and Matrix Formation*

We have only particular harmonic terms due to the symmetry of the problem, all that remains is to determine the coefficient $A_{2n}^{m}$. The residual function $\mathcal{F}(\psi^{2N})$ is obtained by inserting Eq. (15) into Eq. (12)

$$\mathcal{F}(\psi^{2N}) = -\Lambda\psi^{2N} + \beta\Omega\psi^{2N}. \tag{17}$$

If $\psi^{2N}$ were the true solution the residual function would vanish. *Galerkin's principle* is then applied by setting $\mathcal{F}(\psi^{2N})$ orthogonal to each group of spherical harmonics in Eq. (15) over the proper range of $\theta$ and $\phi$. In other words,

$$I[\mathcal{F}(\psi^{2N}) P_{2q}^{p} C_p] = 0, \tag{18}$$

$$(p = 0, 1, \cdots, 2q, \quad q = 1, 2, \cdots, N)$$

We then have $N(N+2)$ systems of equations for the $A_{2q}^{p}$ coefficients.

$$0 = \frac{(1-\epsilon)(2q+p)!}{(2q-p)!(2q+1/2)} \{(2q)(2q+1) A_{2q}^{p}$$

**Table 1. Coefficients of Eq. (19)**

$$a_{n,n+2}^{m,m+1} = \frac{(n+3)(n-m+1)(1+\delta_{m,0})}{2(2n+1)(2n+3)}$$

$$a_{n,n}^{m,m+1} = \frac{(2n^2+2n-3m)(1+\delta_{m,0})}{2(2n-1)(2n+3)}$$

$$a_{n,n-2}^{m,m+1} = \frac{(n-2)(n+m)(1+\delta_{m,0})}{2(2n-1)(2n-1)}$$

$$a_{n,n+2}^{m,m-1} = -\frac{(n+3)(n-m+3)(n-m+2)(n-m+1)(1-\delta_{m,0})}{2(2n+1)(2n+3)}$$

$$a_{n,n}^{m,m-1} = -\frac{(2n^2+2n-3m)(n-m+1)(n+m)(1-\delta_{m,0})}{2(2n+1)(2n+3)}$$

$$a_{n,n-2}^{m,m-1} = -\frac{(n+m-2)(n+m-1)(n+m)(n-2)(1-\delta_{m,0})}{2(2n-1)(2n+1)}$$

* All other $a_{n,k}^{m,j}$ are zero.
* Lower indices should be greater than or equal to upper ones.
* $\delta_{m,0}$ is the Kronecker delta function.

$$+\beta \sum_{n=p/2+1}^{N} \{A_{2n}^{p+1} (\sum_{k=n-1}^{n+1} a_{2n,2k}^{p+1,p} \delta_{q,k})\}$$

$$-\beta \sum_{n=p/2}^{N} \{A_{2n}^{p-1} (\sum_{k=n-1}^{n+1} a_{2n,2k}^{p-1,p} \delta_{q,k})\}$$

$$+\epsilon \sum_{n=p/2+1}^{N} \{A_{2n}^{p} (2n)(2n+1) K_{2n,2q}^{p}\}$$

$$+\epsilon\beta \sum_{n=p/2+1}^{N} \{A_{2n}^{p-1} (\sum_{k=n-1}^{n+1} a_{2n,2k}^{p+1,p} K_{2k,2q}^{p})\}$$

$$+\epsilon\beta \sum_{n=p/2}^{N} \{A_{2n}^{p-1} (\sum_{k=n-1}^{n+1} a_{2n,2k}^{p-1,p} K_{2k,2q}^{p})\}$$

$$(0 \le \epsilon \le 1) \tag{19}$$

where the coefficients $a_{n,k}^{m,j}$ are defined in Table 1, $\delta_{i,j}$ is the Kronecker delta function and all indices are nonnegative integers. The coefficients $K_{2q,2r}^{p}$ are constants which have the general form

$$K_{2q,2r}^{p} = \int_{0}^{1} \int_{-t_o}^{t_o} (P_{2q}^{p} P_{2r}^{p}) \, dt \, dt_o \tag{20}$$

where $t_o$ is defined by $z_c = (1-\epsilon t_o)/2$. Equation (14) provides the following equation for $A_{2q}^{p}$ to make the system determinate:

$$1 = A_0^0 + \frac{\epsilon/2}{1-\epsilon/2} \sum_{n=1}^{N} (K_{0,2n}^{0} A_{2n}^{0}) \quad (0 \le \epsilon \le 1). \tag{21}$$

Thus, the final $[N(N+2)+1] = (N+1)^2$ equations in Eqs. (19) and (21) must be solved simultaneously with the systematic matrix calculation. In case of Poiseuille type external flow, the velocity profile of RD or RR can

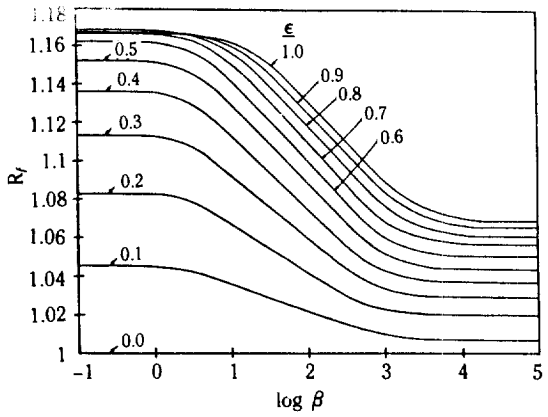


**Fig. 4. Numerical results of the $R_f$ versus log $\beta$ relation for various values of $\epsilon$ in RR model.**

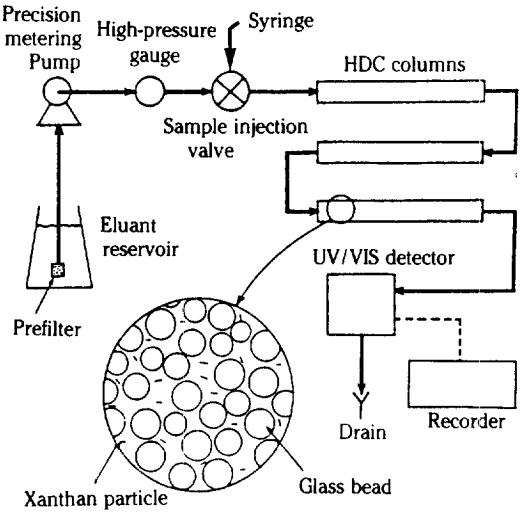


**Fig. 5. Schematic diagram of the HDC experimental setup.**

be easily obtained by arithmetic averaging of the velocities of each mass point. Thus,

$$v_p = v_c\left(\frac{1}{4} - z_c^2 - \gamma\epsilon^2\cos^2\theta\right) \tag{22}$$

where $\gamma$ is the retardation factor, that is, 1/4 for dumbbell (RD) and 1/12 for rod (RR).

4-3. *$R_f$ Equation*

Once distribution function and velocity profile for particles are known, then it is straightforward to obtain the value of $R_f$. The $R_f$ equation of RD (or RR) model polymer can be written in the following

$$R_{f,rig} = 6\int\{\psi(z_c, \theta, \phi)\, v_p(z_c, \theta)\}. \tag{23}$$

After integrating over spacial variables and utilizing the definition of coefficients K's in Eq. (20), we have

$$R_{f,rig} = \frac{1}{1-\epsilon/2}\left\{\left[1-(1/2+2\gamma)\epsilon^2+(1/8+3\gamma/2)\epsilon^3\right]A_0^0 - \epsilon^2\left[(1/5+4\gamma/5)-(1/16+3\gamma/4)\epsilon\right]A_2^0\right\} - \sum_{n=2}^{N}\left[(1/12+\gamma)\left(\frac{\epsilon^3}{1-\epsilon/2}\right)(K_{0,2n}^0+2K_{2,2n}^0)A_{2n}^0\right]. \tag{24}$$

## NUMERICAL COMPUTATION FOR $R_f$ OF RIGID POLYMER MODEL

Very accurate $R_f$ profiles as a function of the logarithmic dimensionless shear rate ($=\log\beta$) for various values of the parameter $\epsilon$ in the range of 0.0 to 1.0 were computed. Assigning the value of retardation factor $\gamma$ in Eq. (24) results in the difference between RD and RR model, and numerical results of RR model from this simulation are presented in Figure 4. Convergence of Galerkin's method insures that with increasing N the resulting solutions $R_f(N,N)$ will converge in the mean toward $R_f$ at every value of $\beta$ provided that a unique exact solution for $R_f$ exists. Computational procedures are repeated until the relative error for the $R_f(N,N)$ is less than the *convergence criteria* given by $0.5\times10^{-6}$. This number of N needed increased with increasing $\beta$, thus for $\log\beta \geq 1.8$, the maximum N value of 15 was used. Computations given here were obtained on an Elxsi-6400 computer using a UNIX OS/BSD operating system. And details of this algorithm are available in Appendix A.

## EXPERIMENTS FOR RIGID ROD MODEL POLYMER

### 1. Apparatus

The basic apparatus, including a detail of the chromatographic column, is shown schematically in Figure 5. An Eldex precision metering pump (Model AA-100-S) which is capable of a maximum flow rate of 10.0 ml/min with continuous downwards to 0.2 ml/min was used to pump the eluant from the reservoir. In order to remove dust and other impure materials that might foul the pump the eluant is filtered twice: once with a 0.5 $\mu$m Millipore filter during preparation, and again with a 2.0 $\mu$m frit located at the pump inlet. The sample is injected into the eluant stream, without interrupting flow to the column, through a Chromatronix 6 port injection valve (7010 RV) with a 1.0 ml sample loop. Three Alltech/Applied Science HPLC columns, 0.6 cm inner diameter by 50 cm long, were packed with spherical glass beads from Potters Inc.. Glass

beads were successively washed with mixed solvents of 0.1M hydrochloric acid, methanol, and acetone, and then dried at 98°C. A solution of acetone in methanol was used for particle dispersion when incorporation of a marker was desired. Particle size distribution of glass beads after sieving as measured on a particle size counter (Micromeritics Inc.) gave the range of 18-30 $\mu$m, and the mean particle diameter of about 23 $\mu$m could be obtained. The bulk density of glass beads had a value of about 2.62 g/cm$^3$. The dry packing of glass beads was performed with Electric Vibro-Engraver (Model V-74, Burgess Vibrocrafters Inc.), and the mean bed porosity of the packed column was 0.353. When eluant and sample come out of the column, they pass into a Waters Series 441 UV/VIS absorbance detector. The polymer and marker species were detected in the effluent by monitoring turbidity at 254 nm. Output signals from the detector was monitored on a strip chart recorder (Cole Parmer Inc.).

**2. Materials**

Note that the proper selection of eluant composition is especially important in chromatographic separations of high molecular weight polymers, for which interaction with the packing is mediated by the eluant. A satisfactory eluant contained 0.002M disodium hydrogen phosphate ($Na_2HPO_4$), 0.05% sodium lauryl sulfate ($C_{12}H_{25}OSO_3Na$), and 0.01M formaldehyde which had an ionic strength of about 0.005M. The pH of this eluant was neutral: adjusted to 7.4-7.6. $1.0 \times 10^{-5}$M sodium dichromate ($Na_2Cr_2O_7 \cdot 2H_2O$) was used as a marker. The RR model polymer studied in this work was biopolymer xanthan. The xanthan gum used was manufactured by fermentation of dextrose with *Xanthomonas campestris* from Sigma Chemical Co. (practical grade), which was diluted to 200 ppm concentration. Interesting rheological properties of xanthan solution possessing a cellulose chain as its backbone structure arise from its ordered helical structure which produces a rigid rod-like conformation [13,15]. Xanthan is rather insensitive to the ionic strength of eluant as compared with other polyelectrolytes and is resistant to the mechanical degradation considerably. Reported molecular weights and the intrinsic viscosities are in the range of $(2\text{-}4) \times 10^6$, $(4\text{-}7) \times 10^3$ cm$^3$/g, respectively [15,18-20].

**3. Experimental Procedure**

After the warming-up operation of about 15-30 min all columns reached the steady state condition. The sample of xanthan solution was mixed with marker and then injected into the valve shown in Figure 5. The adjacent overlap of the sample and marker peaks was encountered frequently, thus we should record the peaks separately. To investigate the particle size effect on the $R_f$ polymer chains of 200 ppm native, i.e., unmodified, xanthan prepared were *degraded by sonication* procedure with Ultrasonic Dismembrator (Model 3000 from Fisher Co.) setting at 180 W power. Sonication times were 5, 10, 20, 30, and 60 min, respectively. The zero shear rate viscosities of native and each of sonicated xanthans were determined by using low-shear capillary viscometer of the Ubbelohde type. In order to examine the flow strength effect on the $R_f$'s of selected xanthan solutions the flow rate was varied in the range of 0.5 to 9.5 ml/min.

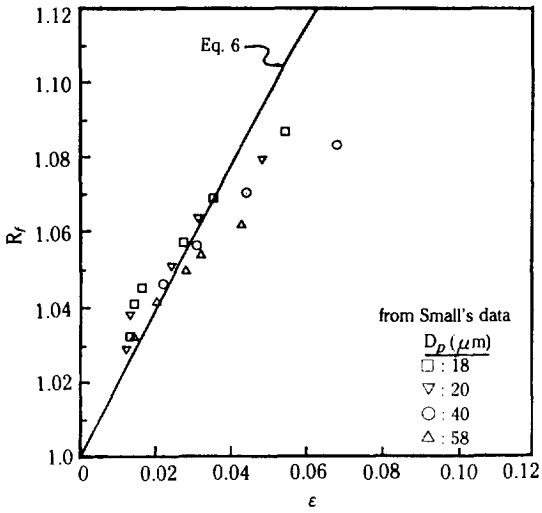


**Fig. 6. A comparison between our theory and experimental results of Small [9] for $R_f$ versus $\epsilon$ relation in SB model.**

## RESULTS AND DISCUSSION

**1. Validity of the SB Model**

For the comparison of our theoretical work with other experimental studies, the Small's previously published data of spherical polystyrene latex with different packing diameters $D_p$ at high ionic strength of $4.6 \times 10^{-3}$M [9,11], was analyzed to display the relationship between $R_f$ and $\epsilon$ in Figure 6. The master curve for $\epsilon$ with different sizes of packing materials, based on several simplifying assumptions, could be constructed. The complex geometry of packing bed is assumed reasonably as a bundle of straight capillary tubes, and in consequence the *equivalent capillary radius* $r_e$ can be estimated from the bed hydraulic radius (cf. Ref. 21) as the relation

$$r_e = \frac{D_p \epsilon_r}{3(1-\epsilon_r)} \quad (25)$$

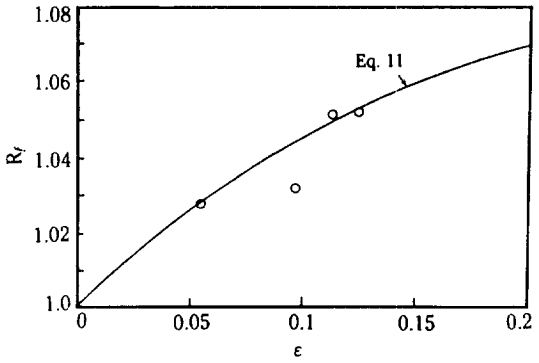


**Fig. 7. A comparison between our theory and experimental results of Prud'homme et al. [13,15] for $R_f$ versus $\epsilon$ relation in ED model.**

where $\epsilon_v$ is the mean bed porosity. For $D_p$ of 18 and 20 $\mu$m each of the $\epsilon_v$ values presented in the above literature were 0.356 and 0.358, but for the cases of $D_p$ of 40 and 58 $\mu$m the $\epsilon_v$ values which were not given in literature were chosen as 0.378 and 0.396, respectively, from a linear relationship between $\epsilon_v$ and $D_p$ resulted in the small particle range. This prediction is meaningful since the $\epsilon_v$'s used are widely accepted ranges for close random dry packing.

A good agreement between theoretical $R_f$ equation and experimental results is found within the small $\epsilon$ region, that is, up to about 0.04. However, there is a growing tendency that the experimental $R_f$ value is smaller than the value evaluated by Eq. (6) with increasing value, and so we feel require another phenomenological explanation. First of all, this behavior is due to the wall effect occurred by the geometrical porous media characteristics of periodically constricted tube, which is considerable in narrow region of space. Next, it must be pointed out that hydrodynamic force is the only matter of concern at this work. Hence, we should necessarily keep in mind the role of *colloidal forces* and the *surface adsorption* of particles, which may cause the critical influence.

## 2. ED Model for Flexible Polymer

A theoretical prediction of Eq. (11)and the experimental results deduced from a series of articles by Prud'homme et al. [13,15] were compared in Figure 7. Prud'homme et al. carried out experiments on the characterization of partially hydrolyzed polyacrylamide which is a flexible linear-chain coil. In Figure 7, despite of the somewhat unclear fitness, the agreement between the theoretical and experimental studies of linear ED model can be said acceptable. It is the same behavior to SB model that the $R_f$ increases with increasing the $\epsilon$ which is defined as $\epsilon = 1/a = \sqrt{(2kT/H)}/l$. In particular, it is noted that this result of ED model does not include the flow effect on Flexible polymer chains as mentioned in the theoretical part [see Eqs. (9),(11)]. The flexible chain structure in flow fields makes the analysis of this model more complicated since the *onset* of deformation in flow is observed. Hence, we recommend that spring force constant H owing to the elastic characteristic of this model polymer should be considered carefully.

## 3. RR Model for Rigid Polymer

The RR model can be treated as a multibead model with infinitely large numbers of beads, and we know that it should have identical distribution function to that of RD model if the beads are equispaced and mass of the polymer is equally distributed in each bead, where every bead is of point mass. Therefore, it turns out to be identical to that of RD without retardation, the difference only arises when the retardation of polymer velocity is concerned. As mentioned before, RR has only one-third retardation of that of RD.

Degraded xanthan molecules are characterized by measuring intrinsic viscosity and the $R_f$, whose viscometric properties are quite consistent with those of relatively rigid rods. It is well known that the molecular weight of xanthan decreases owing to the chain scission mechanism by sonication for increasing lengths of time. The value of intrinsic viscosity for a linear polymer in a specific solvent is related to the polymer molecular weight through the familiar Mark-Houwink relation. Unfortunately, however, there is not a clear-cut answer to the question of the xanthan conformation or the above relation. To calculate the weight-average molecular weight of xanthan Mw for this research, we set up the following very reliable equations:

$$[\eta] = \begin{cases} 3.7731 \times 10^{-6} \cdot Mw^{1.431} & \text{(26a)} \\ \text{(for below } [\eta] \sim 200, \text{ i.e., } Mw \sim 2.5 \times 10^5) & \\ 6.7640 \times 10^{-6} \cdot Mw^{1.384} & \text{(26b)} \\ \text{(for } 200 \sim [\eta] \sim 1000, \text{ i.e., } 2.5 \times 10^5 \sim Mw \sim 10^6) & \\ 5.4587 \times 10^{-4} \cdot Mw^{1.061} & \text{(26c)} \\ \text{(for above } [\eta] \sim 1000, \text{ i.e., } Mw \sim 10^6) & \end{cases}$$

where each Mark-Houwink constant was evaluated from literature information [18-20]. The decreasing tendency of the exponent of Mw suggested that this molecule should not be completely RR but somewhat flexible. Estimated Mw values from the above Eq. (26) closely agreed with the Yamakawa-Yoshizaki's cor-

**Table 2. Experimental results of the size effect for xanthan on $R_f$**

| Sonication Time for xanthan(min) | $[\eta] \times 10^{-3}$ (ml/g) | $Mw \times 10^{-5}$ (g/mol) | p | $L_{eq}$ ($\mu$m) | $\epsilon$ | $R_f$ |
|---|---|---|---|---|---|---|
| 0 (=native) | 5.34 | 38.775 | 425 | 1.154 | 0.138 | 1.0313 |
| 5 | 2.24 | 17.098 | 262 | 0.640 | 0.077 | 1.0220 |
| 10 | 1.05 | 8.372 | 172 | 0.382 | 0.046 | 1.0183 |
| 20 | 0.32 | 3.511 | 89 | 0.184 | 0.022 | 1.0126 |
| 30 | 0.18 | 2.322 | 65 | 0.129 | 0.015 | 1.0105 |
| 60 | 0.05 | 0.949 | 32 | 0.059 | 0.007 | 1.0040 |

*at flow rate = 1.4 ml/min.

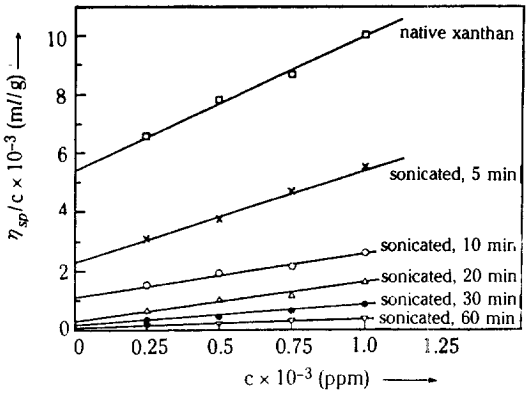


**Fig. 8. The plot of reduced specific viscosity versus concentration as a function of sonication time, at 30°C.**

relation [20] with relative error of under 11%. Intrinsic viscosities $[\eta]$ were obtained at zero concentration by extrapolating the curves of reduced specific viscosity $\eta_{sp}/c$ versus concentration as shown in Figure 8. The reasonable relationship between intrinsic viscosity and macromolecular dimensions for RR particles was predicted for the high values (>50) of length-to-diameter ratio p [18]. These relations between p and viscosity factor $v_o = [\eta]_o/v_{sp}$ can be approximated by the power law function:

$$v_o = 0.159p^{1.801}. \quad (27)$$

Here, $v_{sp}$ is the specific volume, equal to 0.620 for oligosaccharides. The calculation for rods gives p, then the *equivalent length of xanthan* $L_{eq}$ can be estimated from

$$L_{eq}^3 = \frac{45}{2\pi N_A}[\eta]Mw(\ln 2p - 0.5) \quad (28)$$

where $N_A$ is Avogadro's number. The $\epsilon$ can be obtained from the computation of equivalent confined bed radius with Eq. (25). These results are presented in Table 2, where the $R_f$ of xanthan can be seen to increase gradually as $\epsilon$ increases.

**Table 3. Experimental results of the flow rate versus $R_f$ relation for xanthan**

| Run No. | Flow Rate (ml/min) | $R_f$ sonication time for xanthan (min) | | | Shear Rate, Nominal ($sec^{-1}$) |
|---|---|---|---|---|---|
| | | 0 | 10 | 60 | |
| 1 | 0.5 | 1.0380 | 1.0206 | 1.0038 | 798 |
| 2 | 1.0 | 1.0305 | 1.0175 | 1.0042 | 1597 |
| 3 | 2.0 | 1.0240 | 1.0150 | 1.0030 | 3194 |
| 4 | 3.6 | 1.0180 | 1.0127 | 1.0027 | 5749 |
| 5 | 9.5 | 1.0142 | 1.0101 | 1.0033 | 15170 |

*see Figure 9.

## 4. Effect of the Flow Strength on RR Model

By anisotropic, we mean that the angular distribution of the orientations of the rods is not random. $R_f$'s of the three xanthan samples which were native, and sonicated xanthans with 10 min as well as 60 min were determined for the flow rate variations as given in Table 3. Theoretical predictions by numerical simulation for solving Eq. (24) and experimental results marked with data points are illustrated in Figure 9, which agree each other reasonably. Solid lines in the plot are simulated results for many differents of $\epsilon$ and log $\beta$ values. The $R_f$ measurements for exceedingly small flow rate less than 0.1 ml/min were difficult since the required run times were very long (over 24 hr) for this HDC experiment.

From the $R_f$ versus log $\beta$ plot for different $\epsilon$ values of Figure 9, the $R_f$ decreases clearly with increasing flow rate within the range of about log $\beta = 0 \sim 3$. However, in the outside of this region the $R_f$ maintains constant, which is independent of flow rates: i.e., too weak and too strong flow regimes. It can be supposed

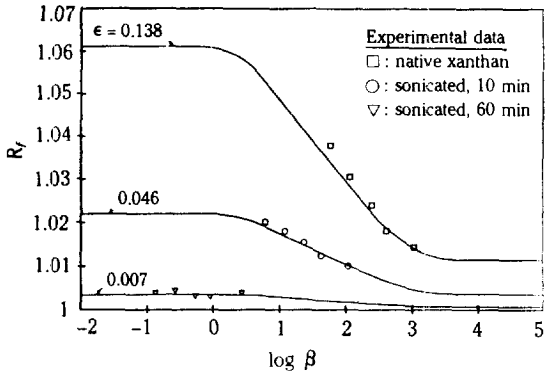


**Fig. 9. Experimental verification on numerical simulations for $R_f$ versus log $\beta$ with different $\epsilon$ values.**

that the deviation behavior of experimental $R_f$ with increasing $\epsilon$ is perhaps caused by a little deformation of xanthan for high Mw (i.e., above Mw ~ $10^6$). Here, the dimensionless shear rate $\beta$ defined in the preceding part corresponds to the rotary Péclet number. Qualitatively, one can conclude that the increasing flow rate causes the rods to align more in the flow direction. This alignment will result in a decreased effective diameter for rod which is equivalent to a characteristic length transverse to the direction of flow. Our approach emphasizes the importance of the *rod orientational distribution* on the microscopic phenomena. In addition, if the flow rate is low enough the maximum effect of separation on RR model would be expected because of its highest $R_f$ value. However, for the efficient separation as well as the reducing of dispersion during HDC operation, another subject to determine the optimum conditions is remained unsolved.

## CONCLUSIONS

The application of HDC as a substitutive technique for high-molecular-weight polymer fractionation, is still in its early stage of development. A theoretical prediction for HDC analysis involving particle size as well as flow effect and its experimental verification have been performed. Main conclusions are as follows.

(1) Flow and dynamic behaviors of polymer in the HDC column have been analyzed and developed quantitatively by introducing the dimensionless separation parameter $R_f$, which could be obtained mathematically from the known distribution function ($\psi$) and velocity profile for particles ($v_p$) under shear flow field.

(2) Good agreements between our theoretical predictions and other researcher's experimental results were found in cases of SB model within the region of rather small $\epsilon$ and ED model. The disagreement in SB model with increasing $\epsilon$ seems to be due to the fact that the main concern of this work was confined to the hydrodynamic effect only. The $R_f$ equation of rigid polymer model was obtained by extending the molecular theory of dilute polymer solutions in a confined geometry to mimic the flow in the porous media HDC column.

(3) The RR model polymer used here was xanthan gum—a slightly flexible rod-like. Despite of several approximations, there was the remarkable agreement between the numerical simulation and experiments. The $R_f$ value showed the gradual increasing behavior with the particle size increased, but revealed a kind of transition with decreasing behavior as the flow strength increased. However, over a certain range (that is about log $\beta < 0$, log $\beta > 3$), the invariant $R_f$ regimes independent of flow rates were observed in particular. This result of flow effect study represented the orientation of the rods in flow. Additionally, for the same flow strength the $R_f$ was higher as the $\epsilon$ was larger.

## Appendix A: Algorithm for Numerical Solution

The present work is undertaken to calculate the full set of $R_f$ values for rigid polymer as functions of size ($\epsilon$) and flow strength ($\beta$) by solving Eq. (24). In order to increase the accuracy as much as possible all solutions are computed in double precision (64-bit), and the general algorithm of the program is as follows.

First of all, the main program HDCRF reads as input data the following: sk(ip,iq,ir), $\epsilon$, $\beta$, and N. Here, the sk(ip,iq,ir) denote the coefficients $K^p_{2q,2r}$ which exist in the data file SKOUT_DAT evaluated by running the program SKCOMP. The program SKCOMP calls on the subroutine QUAD2D to integrate a supplied function FUNCT over a two-dimensional space and should require two copies of a one-dimensional integrator estimated by using 24-point Gauss-Legendre quadrature formula. The FUNCT calls on the function PN which computes the associated Legendre polynomial $P^m_{2n}$ based on the stable recurrence involving subscript 2n. Next, the HDCRF should solve $(N+1)^2$ equations for Eqs. 19 and 21 simultaneously, and the following matrix form is built up:

$$[\mathbf{X}] \times [\mathbf{A}] = [\mathbf{B}] \qquad \text{A1}$$

$$\begin{bmatrix} x_{1,1} & x_{1,2} & \cdots & x_{1,N+1} \\ x_{2,1} & \ddots & & \vdots \\ \vdots & & \ddots & \vdots \\ \vdots & & & \vdots \end{bmatrix} \times \begin{bmatrix} a_1 (= A^0_0) \\ a_2 (= A^0_2) \\ a_3 (= A^1_2) \\ a_4 (= A^2_2) \end{bmatrix} = \begin{bmatrix} 1 \\ 0 \\ 0 \\ 0 \end{bmatrix}$$

$$\begin{bmatrix} \vdots & \vdots \\ x_{N+1,1} \cdots\cdots & x_{N+1,N+1} \end{bmatrix} \begin{bmatrix} \vdots \\ a_{N+1} \end{bmatrix} = \begin{bmatrix} \vdots \\ 0 \end{bmatrix}$$

where [**A**] and [**B**] are (N + 1) by 1 column matrices. Note that the [**B**] matrix is a so-called unit column matrix. In this step, computations of sk and sa variables are achieved by reading the SKOUT_DAT as well as by calling on the function SA. Solutions of the above matrix equation for an unknown set of vectors [**A**] (that is, $A_0^0$, $A_2^0$, $A_2^1$, $A_2^2$, $A_4^0$,···) are performed with calculations of the matrix [$\mathbf{X}^{-1}$] which is the matrix inverse of a square matrix [**X**] of order (N + 1) by calling on the subroutines LUDMAT and FBSMAT (see Ref. 22, Ch.2). In both LUDMAT and FBSMAT, the matrix [**X**] is decomposed into lower and upper triangulars and then is solved exactly by forward and back substitutions. The number of N can be extended to rather large value. The limiting factor is only the available memory size, not accuracy or even running time.

## ACKNOWLEDGEMENT

This research was supported by the Korea Science and Engineering Foundation. Authors gratefully acknowledge financial support from the KOSEF.

## NOMENCLATURE

$A_{2n}^m$ : coefficients of distribution function solution
a : reciprocal dimensionless length scale
a′ : reciprocal characteristic length scale of ED
$a_{n,k}^{m,j}$ : coefficients of Eq. (19), defined in Table 1
C : concentration distribution
$C_m$ : abbreviation for $\cos(m\phi)$
$C_1$ : constant of Eq. (9) in dimensionless coordinates
c : polymer concentration
D : capillary or column diameter
$D_p$ : packing diameter
$D_r$ : rotational diffusivity
d : particle diameter
$\mathcal{F}$ : residual function
H : spring force constant
I : normalization operator
$K_{2q,2r}^p$ : a function defined by Eq. (20)
k : Boltzmann constant
L : length of RR, or RD connector
$L_{eq}$ : equivalent xanthan length
$l$ : spacing between the parallel plates
Mw : weight-average molecular weight
N : integer variable for order of approximation to $\psi$
$N_A$ : Avogadro's number
$P_{2n}^m$ : associated Legendre polynomial
p : length-to-diameter ratio
$R_f$ : retention factor
r : radial axis
$\vec{r}$ : configuration vector of RD
$\vec{r}_1$, $\vec{r}_2$, $\vec{r}_c$ : position vector
$r_e$ : equivalent capillary radius
T : absolute temperature
t : time
$t_m$ : eluant elution time
$t_o$ : $(1-2z_c)/\epsilon$
$t_p$ : particle elution time
$V_m$ : average eluant velocity determined by $t_m$
$V_p$ : average particle velocity determined by $t_p$
$\vec{v}$ : velocity vector
$v_c$ : constant velocity defined by quadruple of the maximum velocity
$v_o$ : viscosity factor
$v_m$ : local eluant velocity
$v_p$ : local particle velocity
$v_{sp}$ : specific volume
x,y,z : the element of configuration vector of $\vec{r}$
$z_c$ : center of mass Z coordinate of polymer

### Greek Letters

$\alpha$ : velocity gradient
$\beta$ : dimensionless velocity gradient
$\gamma$ : retardation factor
$\delta_{ij}$ : Kronecker delta
$\epsilon$ : dimensionless length scale
$\epsilon_v$ : mean bed porosity
$\zeta$ : friction coefficient of bead
$\eta_{sp}/c$ : reduced specific viscosity
$[\eta]$ : intrinsic viscosity
$[\eta]_o$ : Newtonian intrinsic viscosity
$\theta$, $\phi$ : polar, and azimuth angles defining the orientation of $\vec{r}$
$\lambda$ : relaxation time constant for RD
$\Lambda$ : spherical operator
$\psi$ : nondimensionalized distribution function
$\psi^{2N}$ : Nth order of approximation to $\psi$
$\psi_{eq}$ : nondimensionalized equilibrium distribution function
$\Omega$ : convective operator

### Superscript

m,p : upper index with integers

**Subscript**

k,n,q : lower index with integers

## REFERENCES


1. Bird, R.B., Curtiss, C.F., Armstrong, R.C. and Hassager, O.: "Dynamics of Polymeric Liquids, Vol. 1. Fluid Mechanics, Vol. 2. Kinetic Theory", Wiley, New York (1987).
2. Stewart, W.E. and Sorensen, J.P.: *Trans. Soc. Rheol.*, **16,** 1 (1972).
3. Aubert, J.H. and Tirrell, M.: *J. Chem. Phys.*, **72,** 2694 (1980).
4. Stasiak, W. and Cohen, C.: *J. Chem. Phys.*, **78,** 553 (1983).
5. Park, O.O. and Fuller, G.G.: *J. Non-Newtonian Fluid Mech.*, **15,** 309 (1984).
6. Park, O.O.: Ph.D. Thesis, Stanford University (1985).
7. DiMarzio, E.A. and Guttman, C.A.: *Macromolecules,* **3,** 131 (1970).
8. Brenner, H. and Gaydos, L.J.: *J. Colloid Interface Sci.*, **58,** 312 (1977).
9. Small, H.: *J. Colloid Interface Sci.*, **48,** 147 (1974).
10. Prieve, D.C. and Hoysan, P.M.: *J. Colloid Interface Sci.*, **64,** 201 (1978).
11. Silebi, C.A. and McHugh, A.J.: *AIChE J.*, **24,** 204 (1978).
12. Silebi, C.A. and Dosramos, J.G.: *J. Colloid Interface Sci.*, **130,** 14 (1989).
13. Hoagland, D.A., Larson, K.A. and Prud'homme, R.K.: "HDC Separations of High Molecular Weight Water Soluble Polymers", in Modern Methods of Particle Size Analysis, Howard Barth (ed.), *ACS Symposium Series* (1983).
14. Larson, K.A. and Prud'homme, R.K.: *J. Colloid Interface Sci.*, **96,** 112 (1984).
15. Hoagland, D.A. and Prud'homme, R.K.: *Macromolecules,* **22,** 775 (1989).
16. Yau, W.W., Kirkland, J.J. and Bly, D.D.: "Modern Size-Exclusion Liquid Chromatography-Practice of Gel Permeation and Gel Filtration Chromatography", Wiley, New York (1979).
17. Aubert, J.H. and Tirrell, M.: *J. Chem. Phys.*, **77,** 553 (1982).
18. Chauveteau, G.: *J. Rheol.*, **26,** 111 (1982).
19. Lecourtier, J. and Chauveteau, G.: *Macromolecules,* **17,** 1340 (1984).
20. Sato, T., Kojima, S., Norisuye, T. and Fujita, H.: *Polymer J.*, **16,** 423 (1984).
21. Dullien, F.A.L.: "Porous Media-Fluid Transport and Pore Structure", Academic Press. New York (1979).
22. Press, W.H., Flannery, B.P., Teukolsky, S.A. and Vetterling, W.T.: "Numerical Recipes", Cambridge University Press (1986).